Optics Letters

Near-octave-spanning breathing soliton crystal in an AlN microresonator

Haizhong Weng,[1] Adnan Ali Afridi,[1] Jia Liu,[2] Jing Li,[1] Jiangnan Dai,[2] Xiang Ma,[2] Yi Zhang,[2] Qiaoyin Lu,[2] Weihua Guo,[2,3] and John F. Donegan[1,4]

[1]School of Physics, CRANN and AMBER, Trinity College Dublin, Dublin 2, Ireland
[2]Wuhan National Laboratory for Optoelectronics and School of Optical and Electronic Information, Huazhong University of Science and Technology, 1037 Luoyu Road, Wuhan 430074, China
[3]e-mail: guow@mail.hust.edu.cn
[4]e-mail: jdonegan@tcd.ie

Received 16 February 2021; revised 28 May 2021; accepted 10 June 2021; posted 11 June 2021 (Doc. ID 422842); published 14 July 2021

The soliton crystal (SC) was recently discovered as an extraordinary Kerr soliton state with regularly distributed soliton pulses and enhanced comb line power spaced by multiples of the cavity free spectral ranges (FSRs), which will significantly extend the application potential of microcombs in optical clock, signal processing, and terahertz wave systems. However, the reported SC spectra are generally narrow. In this Letter, we demonstrate the generation of a breathing SC in an aluminum nitride (AlN) microresonator (FSR ∼374 GHz), featuring a near-octave-spanning (1150–2200 nm) spectral range and a terahertz repetition rate of ∼1.87 THz. The measured 60 fs short pulses and low intensity–noise characteristics confirm the high coherence of the breathing SC. Broadband microcombs with various repetition rates of ∼0.75, ∼1.12, and ∼1.5 THz were also realized in different microresonators of the same size. The proposed scheme shows a reliable design strategy for broadband soliton generation with versatile dynamic control over the comb line spacing.

https://doi.org/10.1364/OL.422842

Since dissipative Kerr solitons (DKSs) were first demonstrated in an MgF_2 microresonator [1] through careful balancing of Kerr nonlinearity and dispersion, a great number of researchers have been committed to producing soliton microcombs in various platforms such as silica [2], Si_3N_4 [3–7], AlN [8], $LiNbO_3$ [9,10], and AlGaAs [11]. Due to the merits of miniaturization, high coherence, a broadband spectral range, and a repetition rate in the microwave regime, soliton combs are promising for a wide range of applications such as optical clocks, frequency synthesizers, coherent communications, optical neural networks, and microwave photonics [12–15]. Subsequently, emerging novel soliton types such as breather solitons [16], Stokes solitons [17], and soliton molecules [18] were also demonstrated in diverse microresonators.

The soliton crystal (SC) is a specific soliton state with clearly discrete comb lines spaced by multiple cavity free spectral ranges (FSRs) [19–21]. Such SCs are typically formed in the presence of avoided mode crossing, which induces a modulation on the intracavity continuous-wave background, leading to interference between the solitons [20]. Among the variety of SC states, the perfect soliton crystal (m-PSC) is one ideal representative, which has m pulses uniformly distributed in the cavity [22]. In contrast to a single soliton, the PSCs feature high conversion efficiency and m^2 enhanced comb power. Despite an apparent similarity of the PSC states to primary combs, the former are periodically spaced solitons, while the latter appears to be a modulated continuous wave, rather than a periodic train of solitons [23]. In addition, the primary combs are typically generated under the condition of less pump-cavity detuning, thus limiting the spectral range. As revealed in [22,24], a relatively low pump power is helpful to access the PSCs which, in turn, may restrict the spectral bandwidth. Recently, it was shown that the versatile PSC states can be generated in the $LiNbO_3$ microring resonators (MRRs) and switched by tuning the pump frequency in a bi-directional way due to its intrinsic photorefractive effect [25]. As far as we know, the broadest PSC (1380–1870 nm) in the near-infrared regime was formed in a Si_3N_4 MRR with an FSR of ∼1 THz [22].

Due to the strong Kerr (χ^3) and Pockels (χ^2) nonlinearities, high Q AlN MRRs were employed to produce broadband microcombs and Kerr solitons [8,26–29], as well as the near-visible microcombs [30] and Pockels solitons [31]. Most recently, we have realized the direct accessing of an octave-spanning single DKS in an optimally designed AlN MRR [32], which will eliminate the complicated control or extra equipment often required for soliton behavior.

In this Letter, we experimentally demonstrate the deterministic generation of a near-octave-spanning (1150–2200 nm) breathing SC and the microcombs with adjustable repetition rates in AlN MRRs due to the mode interactions. The high

intrinsic Q factor (Q_{int}), low anomalous dispersion, and pulley-waveguide coupling together promote the formation of the almost octave-spanning microcombs, whose repetition rate can be switched from ~1.5 to ~0.75 THz.

As in the schematic diagram presented in Fig. 1(a), microcombs with discretely adjustable frequency spacing can be excited in different AlN MRRs of the same size, coupled with a straight or pulley-waveguide. The devices are patterned from a 1.2 μm thick epitaxial AlN film on sapphire via standard photolithography and inductively coupled plasma etching processes [33]. In this Letter, we use MRRs with a radius of 60 μm (FSR ~374 GHz) and a cross section of 2.29 μm^2 × 1.2 μm^2 (fully etched), which are designed to ensure a low anomalous dispersion of the target fundamental transverse electric (TE_{00}) mode [32]. The bus waveguide width W and coupling gap G were designed to vary slightly from device to device (see Table S1 in Supplement 1) to optimize the phase-matching condition and improve the extraction efficiency of the microcomb. Figure 1(b) shows the transmission spectrum of a straight-waveguide coupled-resonator 1 ($W = 0.91$ μm, $G = 0.5$ μm) with an insertion loss of 6.4 dB. The TE_{00} and first-order TE (TE_{10}) modes close to each other near 1550.7 nm ($\mu = 5$), accompanied by the significantly changed linewidths and extinction ratios at $\mu = 4$, illustrate a weak coupling between the two transverse modes. The normalized TE_{00} resonance at 1565.73 nm ($\mu = 0$), used for SC generation, is depicted in Fig. 1(d) with a loaded Q factor (Q_{load}) and Q_{int} of 5.2×10^5 and 1.3×10^6, corresponding to a propagation loss of 0.28 dB/cm.

Figure 2(a) shows the simulated TE mode FSRs by solving the eigenfrequencies with the finite element method. The open circles and triangle symbols correspond to the experimental FSRs of the TE_{00} and the TE_{10} modes, which agree with the simulation results very well. The normal and anomalous dispersion regimes are marked by the dashed lines and arrows. The frequency separations between TE_{10} and its nearest TE_{00} resonances were also extracted and plotted in Fig. 2(b). The simulated and measured mode crossing position at the C-band is 1553.6 and 1550.7 nm, respectively. We can expect that the mode crossing will also occur around 1226, 1400, 1701, 1856, and 2034 nm.

To produce the SC, we coupled 250 mW of power into the bus waveguide of resonator 1 and scanned the laser wavelength across the TE_{00} resonance at 1565. 7 nm at a speed of 1 nm/s. A triangular resonance shape was recorded [see the inset of Fig. 3(a)] with several step structures, indicating different comb states. At the marked detuning positions (i)–(iv), we observe the formation of a primary comb, modulation instability (MI) comb, disordered SC, and breathing 5-SC states in sequence. Corresponding optical spectra, radio-frequency (RF) spectra, and autocorrelation (AC) pulse traces are summarized in Figs. 3(a)–3(c). The SCs occur in the final step of the transmission and have a much wider spectral range (1150–2200 nm) than those of the primary and MI comb due to the mode locking and the presence of the dispersive wave emission at ~1200 nm. The disordered SC at state iii is a crystallization procedure related to the passage through an unstable soliton breathing stage [22]. The breathing SC at state iv has a comb line spacing of 5 × FSR (~1.87 THz), while all the other comb lines are suppressed significantly, suggesting a high regularity of the soliton pulse arrangement and the absence of defects. Some weak intermediate comb lines at −60 dB were observed, implying

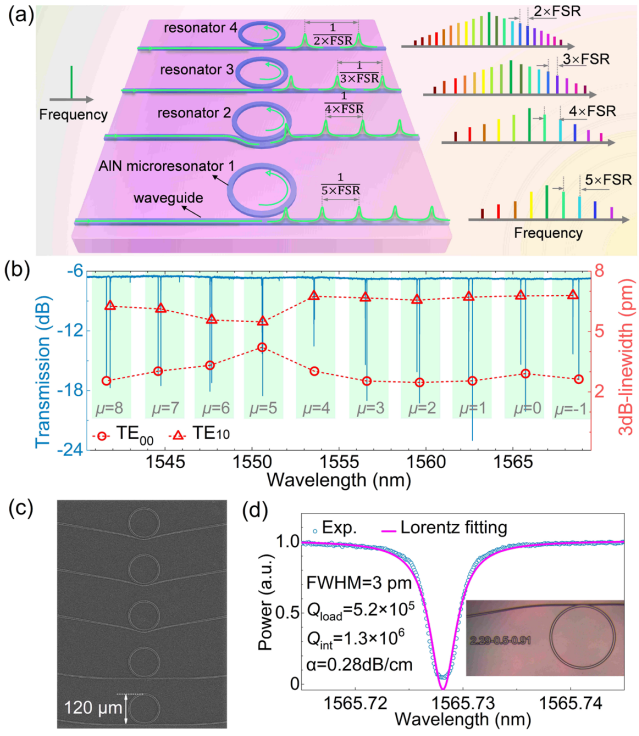

Fig. 1. (a) Schematic diagram of microcombs with adjustable line spacing generated from the AlN MRRs. (b) Cavity transmission at TE polarization. The right-bottom axis indicates the resonance linewidth of the TE_{00} (line + circles) and TE_{10} (line + triangles) modes. Different longitudinal modes with relative mode number μ are marked in the green rectangles. (c) SEM image of the MRR array after dry etching. (d) Resonance profile of TE_{00} mode near 1565.7 nm with Lorentz fitting. Inset: a microscope image of an MRR.

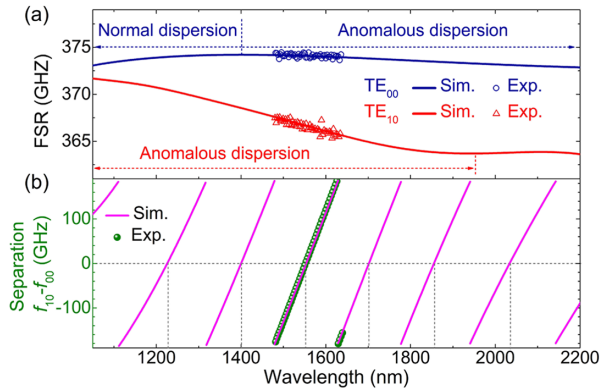

Fig. 2. (a) Experimental and simulated mode FSRs in the designed AlN MRR. (b) Frequency spacing between TE_{00} and the nearest TE_{10} resonances.

that the SC is not perfect. To access the pure PSC, the amplified spontaneous emission noise from the fiber amplifier should be suppressed, and different pump conditions need to be tried for desirable thermal behavior [25]. The 3 dB bandwidth of this breathing SC spectrum is estimated as 8.5 THz via $sech^2$ envelope fitting (gray dashed line), which corresponds to a 38 fs pulse width. The anomaly at ~1401, ~1551, and ~1700 nm is caused by the mode crossing, which is consistent with the simulation results shown in Fig. 2(b).

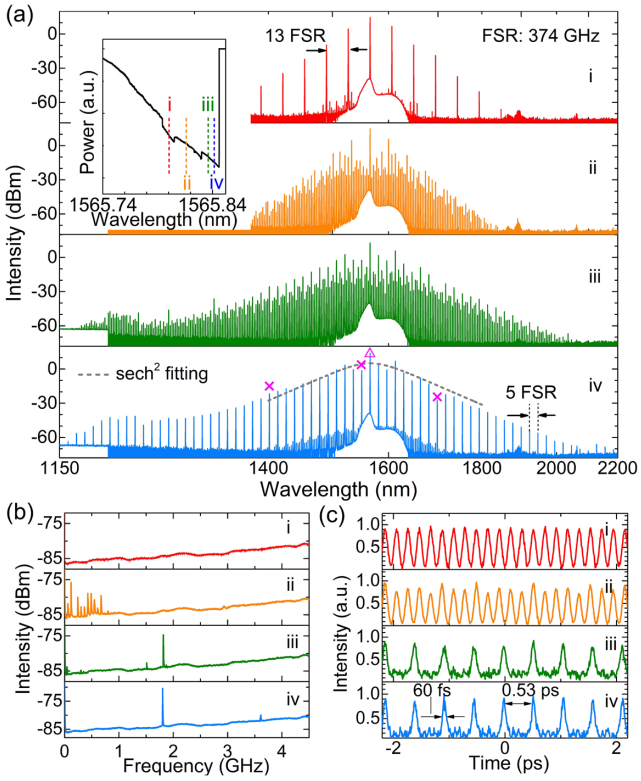

Fig. 3. Breathing SC generation in resonator 1. Inset of (a): cavity transmission at 250 mW. (a) Optical and (b) RF spectral evolutions at the detuning positions (i)–(iv) marked in the transmission. The symbols Δ and × (hereafter) indicate the pump resonance and the mode interaction positions, respectively. (c) Measured AC traces.

Besides the abrupt cavity transmission step, the drastic reduction of the RF noise [see Fig. 3(b)] is further evidence for the transition from chaotic to locked states. In states iii and iv, the RF beat note shows a low-noise background with a sharp tone at ∼1.73 GHz, corresponding to the breathing frequency [16]. The measured breathing frequency has a linear reduction of ∼40 MHz when increasing the effective pump-cavity detuning within a ∼750 MHz range. The relation is consistent or opposite the trends demonstrated in silicon [16] or MgF_2 [34] MRRs. The transition from a stable PSC to a breathing PSC was also investigated in Si_3N_4 microresonators [22]. The breathing frequency can be injection-locked by applying a modulated signal to the pump laser [35]. To further confirm the mode locking, we characterized the temporal characteristics through a second-harmonic generation-based AC measurement. As shown in Fig. 3(c), the AC traces of the primary comb and MI comb are sinusoidal and have a period of 0.2 ps (∝ 13 × FSR). The disordered and breathing SCs have a pulse period of 0.53 ps (∝ 5 × FSR), while the latter one has a higher signal-to-noise ratio and a narrower width of ∼60 fs. The measured pulse width is wider than the estimated value due to our correlator's low responsivity beyond 1600 nm.

We found that the breathing 5-SC can be accessed within an on-chip power range of from ∼230 to ∼275 mW. To achieve a typical single DKS with a repetition rate of 1.87 THz, one would need to exploit a much smaller microring with a radius of 12 μm, which is still challenging due to the large bending losses and limitations on dispersion management in such MRRs. The primary comb results of a 23 μm radius AlN MRR are described in Supplement 1.

In the designed AlN MRRs, the mode interaction near 1550 nm can occur between not only two TE transverse modes, but also the two fundamental modes with different polarizations (see Supplement 1). Considering the slightly different waveguide coupling geometry and the fabrication variations, the MRRs will have similar resonance properties, but different mode interaction positions, giving rise to a possible generation of versatile SCs or repetition-rate-selectable microcombs. Figure 4(a) summarizes the microcomb spectra with line spacing of 2 × FSR, 3 × FSR, and 4 × FSR (0.75, ∼1.12, and ∼1.5 THz), which are produced from the other three MRRs. The ratio between frequency spacing and FSR is tightly linked to the mode interaction position with respect to the pump resonance. For one resonance in the pulley-waveguide coupled-resonator 2, we obtained the near-octave-spanning (1170–2300 nm) microcomb with repetition rates of 4 × FSR (i) and 2 × FSR (ii). The dips near 1354 nm (∼220 THz) in the comb profiles result from the antiphase-matched frequencies [36] because of the pulley coupling, which was demonstrated to

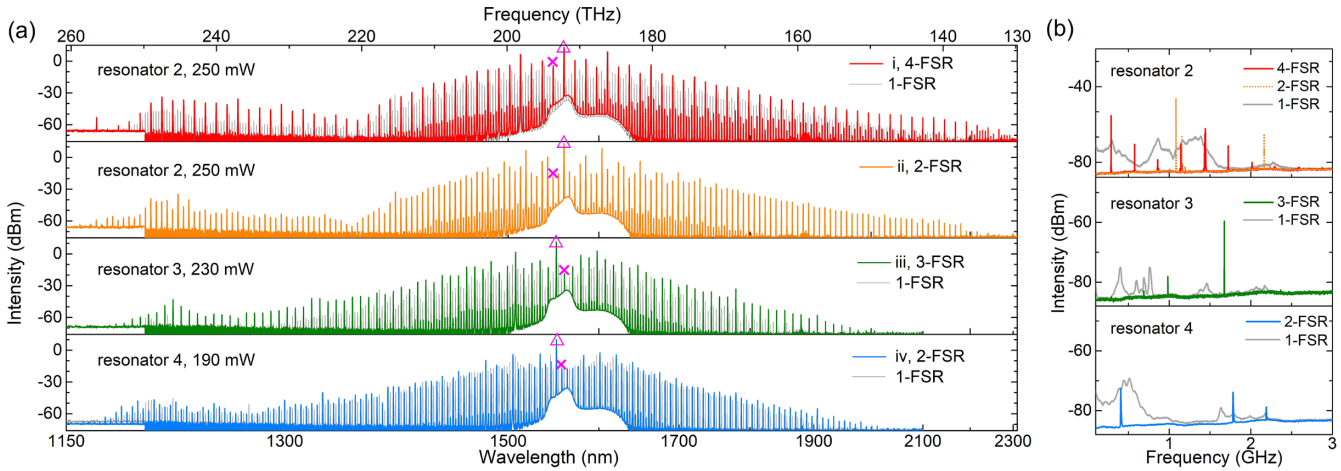

Fig. 4. (a) Optical spectra of the microcombs with frequency spacing of (i) 4 × FSR and (ii) 2 × FSR from the same resonance in resonator 2, (iii) 3 × FSR in resonator 3, and (iv) 2 × FSR in resonator 4. The gray spectra are the microcombs with single-FSR spacing. The symbols Δ and × indicate the pump resonance and the mode interaction position, respectively. (b) RF spectra of the microcombs in (a).

improve the extraction efficiency of the microcombs at a short wavelength compared to the straight coupling.

Moreover, a wider coupling gap G of 600 nm was utilized to increase the coupling efficiency at a long wavelength [28]. Therefore, the microcomb spectra generated from resonator 2 are wider than the spectra (1180-2000 nm) obtained from the straight-waveguide coupled-resonators 3 and 4. As shown in Fig. 4(b), strong RF peaks have been observed for the multiple-FSR microcombs while the single-FSR microcombs have a broadband beat note noise. Considering the insufficiently smooth spectra, we would claim that these microcombs spaced by integer harmonics of the cavity FSR are in the MI state, but with relatively low noise. We noted that these spectra are similar to the measured disordered SC in [20], which has varied comb peak distributions without any apparent regular order. Further simulations and experiments are needed to explore the diverse SCs in the AlN MRRs and achieve the fully mode-locking PSCs.

In summary, we have demonstrated a near-octave-spanning (1150–2200 nm) breathing SC with a repetition rate of ∼1.87 THz in a well-designed AlN microresonator. The coherence of the SCs can be confirmed by the low RF noise and the compressed pulse. The broadband low-noise microcombs with discretely adjustable frequency spacing of ∼0.75, ∼1.12, and ∼1.5 THz were also accessed. The repetition rate can also be altered by simply tuning the pump detuning. Meanwhile, further investigation is needed to realize arbitrarily tunable SC states in a single AlN microresonator or even the same resonance with fewer pump variables.

The demonstration of such near-octave SCs and the low-noise microcombs, with various repetition rates and enhanced comb line power, should significantly extend the potential applications in a quantum regime [37] and photonic convolutional accelerator [15], as well as in terahertz imaging or spectroscopy. For the applications that required self-referencing, the high repetition rate can be detected by combining the soliton microcombs with an electro-optic comb system modulated at tens of gigahertz [13,38]. Additionally, there is also an ambitious vision to realize the self-referenced soliton microcombs in a single AlN chip by combining the Pockels and Kerr nonlinearities [29].

Funding. Science Foundation Ireland (17/NSFC/4918); National Natural Science Foundation of China (61861136001).

Disclosures. The authors declare no conflicts of interest.

Data Availability. Data underlying the results presented in this paper are not publicly available at this time but may be obtained from the authors upon reasonable request.

Supplemental document. See Supplement 1 for supporting content.

REFERENCES

1. T. Herr, V. Brasch, J. D. Jost, C. Y. Wang, N. M. Kondratiev, M. L. Gorodetsky, and T. J. Kippenberg, Nat. Photonics **8**, 145 (2014).
2. X. Yi, Q.-F. Yang, K. Y. Yang, M.-G. Suh, and K. Vahala, Optica **2**, 1078 (2015).
3. V. Brasch, M. Geiselmann, T. Herr, G. Lihachev, M. H. P. Pfeiffer, M. L. Gorodetsky, and T. J. Kippenberg, Science **351**, 357 (2016).
4. C. Joshi, J. K. Jang, K. Luke, X. Ji, S. A. Miller, A. Klenner, Y. Okawachi, M. Lipson, and A. L. Gaeta, Opt. Lett. **41**, 2565 (2016).
5. Q. Li, T. C. Briles, D. A. Westly, T. E. Drake, J. R. Stone, B. R. Ilic, S. A. Diddams, S. B. Papp, and K. Srinivasan, Optica **4**, 193 (2017).
6. M. H. P. Pfeiffer, C. Herkommer, J. Liu, H. Guo, M. Karpov, E. Lucas, M. Zervas, and T. J. Kippenberg, Optica **4**, 684 (2017).
7. X. Ji, J. K. Jang, U. D. Dave, M. Corato-Zanarella, C. Joshi, A. L. Gaeta, and M. Lipson, Laser Photonics Rev. **15**, 2000353 (2021).
8. Z. Gong, A. Bruch, M. Shen, X. Guo, H. Jung, L. Fan, X. Liu, L. Zhang, J. Wang, J. Li, J. Yan, and H. X. Tang, Opt. Lett. **43**, 4366 (2018).
9. Y. He, Q.-F. Yang, J. Ling, R. Luo, H. Liang, M. Li, B. Shen, H. Wang, K. Vahala, and Q. Lin, Optica **6**, 1138 (2019).
10. Z. Gong, X. Liu, Y. Xu, and H. X. Tang, Optica **7**, 1275 (2020).
11. G. Moille, L. Chang, W. Xie, A. Rao, X. Lu, M. Davanço, J. E. Bowers, and K. Srinivasan, Laser Photonics Rev. **14**, 2000022 (2020).
12. T. J. Kippenberg, A. L. Gaeta, M. Lipson, and M. L. Gorodetsky, Science **361**, eaan8083 (2018).
13. T. E. Drake, T. C. Briles, J. R. Stone, D. T. Spencer, D. R. Carlson, D. D. Hickstein, Q. Li, D. Westly, K. Srinivasan, S. A. Diddams, and S. B. Papp, Phys. Rev. X **9**, 031023 (2019).
14. E. Lucas, P. Brochard, R. Bouchand, S. Schilt, T. Südmeyer, and T. J. Kippenberg, Nat. Commun. **11**, 374 (2020).
15. X. Xu, M. Tan, B. Corcoran, J. Wu, A. Boes, T. G. Nguyen, S. T. Chu, B. E. Little, D. G. Hicks, R. Morandotti, A. Mitchell, and D. J. Moss, Nature **589**, 44 (2021).
16. M. Yu, J. K. Jang, Y. Okawachi, A. G. Griffith, K. Luke, S. A. Miller, X. Ji, M. Lipson, and A. L. Gaeta, Nat. Commun. **8**, 14569 (2017).
17. Q.-F. Yang, X. Yi, K. Y. Yang, and K. Vahala, Nat. Phys. **13**, 53 (2016).
18. W. Weng, R. Bouchand, E. Lucas, E. Obrzud, T. Herr, and T. J. Kippenberg, Nat. Commun. **11**, 2402 (2020).
19. P. Del'Haye, A. Coillet, W. Loh, K. Beha, S. B. Papp, and S. A. Diddams, Nat. Commun. **6**, 5668 (2015).
20. D. C. Cole, E. S. Lamb, P. Del'Haye, S. A. Diddams, and S. B. Papp, Nat. Photonics **11**, 671 (2017).
21. W. Wang, Z. Lu, W. Zhang, S. T. Chu, B. E. Little, L. Wang, X. Xie, M. Liu, Q. Yang, L. Wang, J. Zhao, G. Wang, Q. Sun, Y. Liu, Y. Wang, and W. Zhao, Opt. Lett. **43**, 2002 (2018).
22. M. Karpov, M. H. Pfeiffer, H. Guo, W. Weng, J. Liu, and T. J. Kippenberg, Nat. Phys. **15**, 1071 (2019).
23. Z. Qi, S. Wang, J. Jaramillo-Villegas, M. Qi, A. M. Weiner, G. D'Aguanno, T. F. Carruthers, and C. R. Menyuk, Optica **6**, 1220 (2019).
24. T. Huang, J. Pan, Z. Cheng, G. Xu, Z. Wu, T. Du, S. Zeng, and P. P. Shum, Phys. Rev. A **103**, 023502 (2021).
25. Y. He, J. Ling, M. Li, and Q. Lin, Laser Photonics Rev. **14**, 1900339 (2020).
26. X. Liu, C. Sun, B. Xiong, L. Wang, J. Wang, Y. Han, Z. Hao, H. Li, Y. Luo, J. Yan, T. Wei, Y. Zhang, and J. Wang, ACS Photonics **5**, 1943 (2018).
27. Y. Zheng, C. Sun, B. Xiong, L. Wang, J. Wang, Y. Han, Z. Hao, H. Li, J. Yu, Y. Luo, J. Yan, T. Wei, Y. Zhang, and J. Wang, in *Conference on Lasers and Electro-Optics* (2020), paper SW4J.3.
28. H. Weng, J. Liu, A. A. Afridi, J. Li, J. Dai, X. Ma, Y. Zhang, Q. Lu, J. F. Donegan, and W. Guo, Opt. Lett. **46**, 540 (2021).
29. X. Liu, Z. Gong, A. W. Bruch, J. B. Surya, J. Lu, and H. X. Tang, "III-nitride nanophotonics for beyond-octave soliton generation and self-referencing," arXiv:2012.13496 (2020).
30. X. Guo, C.-L. Zou, H. Jung, Z. Gong, A. Bruch, L. Jiang, and H. X. Tang, Phys. Rev. Appl. **10**, 014012 (2018).
31. A. W. Bruch, X. Liu, Z. Gong, J. B. Surya, M. Li, C.-L. Zou, and H. X. Tang, Nat. Photonics **15**, 21 (2021).
32. H. Weng, J. Liu, A. A. Afridi, J. Li, J. Dai, X. Ma, Y. Zhang, Q. Lu, J. F. Donegan, and W. Guo, Photonics Res. **9**, 1351 (2021).
33. J. Liu, H. Weng, A. A. Afridi, J. Li, J. Dai, X. Ma, H. Long, Y. Zhang, Q. Lu, J. F. Donegan, and W. Guo, Opt. Express **28**, 19270 (2020).
34. E. Lucas, M. Karpov, H. Guo, M. Gorodetsky, and T. J. Kippenberg, Nat. Commun. **8**, 736 (2017).
35. S. Wan, R. Niu, Z.-Y. Wang, J.-L. Peng, M. Li, J. Li, G.-C. Guo, C.-L. Zou, and C.-H. Dong, Photonics Res. **8**, 1342 (2020).
36. G. Moille, Q. Li, T. C. Briles, S.-P. Yu, T. Drake, X. Lu, A. Rao, D. Westly, S. B. Papp, and K. Srinivasan, Opt. Lett. **44**, 4737 (2019).
37. M. A. Guidry, D. M. Lukin, K. Y. Yang, R. Trivedi, and J. Vučković, "Quantum optics of soliton microcombs," arXiv:2103.10517 (2021).
38. S.-P. Yu, D. C. Cole, H. Jung, G. T. Moille, K. Srinivasan, and S. B. Papp, Nat. Photonics **15**, 461 (2021).